Chemical Science

ROYAL SOCIETY OF CHEMISTRY

EDGE ARTICLE

View Article Online
View Journal | View Issue



Cite this: *Chem. Sci.*, 2025, **16**, 9934

All publication charges for this article have been paid for by the Royal Society of Chemistry

Received 21st February 2025
Accepted 18th April 2025

DOI: 10.1039/d5sc01395j

rsc.li/chemical-science



# Alkali metal salts of 1,2,3-benzodiazaborines: platforms for late-stage *N*-functionalization and metal complexation†

Leonie Wüst,[ab] Lea Scheuring,[ab] Tim Wellnitz,[ab] Krzysztof Radacki [ab] and Holger Braunschweig *[ab]

The standard procedure for the preparation of benzoid 1,2,3-diazaborines (DABs) is the condensation of 2-formylphenyl boronic acid with a hydrazine. The choice of hydrazine derivative irreversibly predetermines the *N*-substituent in most cases and is additionally limited by the availability and hazardous nature of the respective hydrazines. Options to subsequently modify the *N*-substituent are scarce. Herein, we explore an approach to postsynthetic *N*-functionalization *via* isolable, nucleophilic DAB alkali metal amides. The structures of these metalated DABs were extensively studied, utilizing $^{1}$H DOSY NMR spectroscopy and XRD analysis. Subsequent reactivity studies of these unusual amides revealed an intricate, dualistic reactivity pattern. Upon treatment with mild electrophiles, the DAB amides react as *N*-nucleophiles, facilitating the straightforward introduction of functional groups at the $N_\alpha$ position. Due to the incorporation of the second $N_\beta$ atom, they can moreover serve as anionic diazo ligands for the formation of μ-DAB-bridging coinage metal complexes, which bear a striking resemblance to well-studied complexes with pyrazolato ($pz^-$) ligands. Overall, this work demonstrates how BN incorporation opens new avenues in ligand design and provides a valuable tool for post-synthetic modification of aryl DABs with organic and inorganic substrates.

## Introduction

Traditionally, organic and inorganic chemistry have been considered distinct sub-disciplines, with the former focusing on carbon-based compounds and the latter encompassing the remaining elements of the periodic table. However, certain compounds defy this clinical separation of fields and captivate both organic and inorganic chemists alike. A prime example that bridges this divide is borazine ($B_3N_3H_6$), which was first synthesized by Stock and Pohland in 1926 and is often referred to as "*inorganic benzene*".[1,2] While borazine and benzene undoubtedly share some similarities such as equalized bond lengths[3] and, based on the CC/BN isosterism, an identical total electron count,[4] the replacement of C=C units with B=N fragments also results in some fundamental differences. Due to the higher polarity of the BN bond, borazine is susceptible to hydrolysis[5] and, in contrast to the model aromatic benzene, considered only weakly aromatic at best.[6,7] The isoelectronic replacement of a single C=C unit in benzene with a B=N unit yields 1,2-azaborines, which impressively demonstrate another striking disparity to their all-carbon counterparts: the introduced dipole moment enables the formation of N–H hydrogen bonds (Fig. 1a).[8] Interestingly, this drastically alters their biochemical reactivity, *e.g.* by creating additional sites for protein–ligand interactions with enzyme binding pockets.[8,9] Driven by the potential to generate novel pharmacophores through BN-doping, intensive efforts are underway to develop

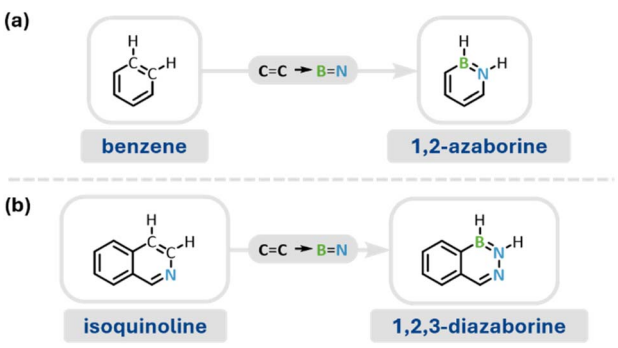


Fig. 1 Isoelectronic relationship of the parent compounds (a) benzene and 1,2-azaborine and (b) isoquinoline and 1,2,3-diazaborine. Note: we refrain from drawing the formal charges for all neutral BN-heterocycles.

[a]*Institute for Inorganic Chemistry, Julius-Maximilians-Universität Würzburg, Am Hubland, 97074 Würzburg, Germany. E-mail: h.braunschweig@uni-wuerzburg.de*

[b]*Institute for Sustainable Chemistry & Catalysis with Boron, Julius-Maximilians-Universität Würzburg, Am Hubland, 97074 Würzburg, Germany*

† Electronic supplementary information (ESI) available: Experimental details and procedures, analytical, computational and supplementary data. CCDC 2425624–2425639. For ESI and crystallographic data in CIF or other electronic format see DOI: https://doi.org/10.1039/d5sc01395j

new synthetic strategies for these intriguing (in)organic heterocycles.[10–12]

Late-stage functionalization subsequent to initial formation of the BN-heterocycles is particularly attractive, as it provides access to diverse molecular scaffolds with reduced synthetic effort. For 1,2-azaborines, late-stage derivatization of the endocyclic N-atom is well established and primarily facilitated by three different methods: (i) direct substitution reactions by deprotonation of the N–H functionality and interception with an appropriate organic or inorganic electrophile,[13–16] (ii) Buchwald–Hartwig amination with C($sp^2$)-substrates[16] and (iii) C(sp)-alkynylation using a Cu(I) catalyst.[16] From a laboratory perspective, method (i) is advantageous, as simple salt metathesis reactions produce easily separable salts as byproducts and do not rely on expensive transition metal catalysts. Building on prior work of Ashe and coworkers,[13,14] our group has successfully isolated nucleophilic alkali metal amides of 1,2-azaborines, enabling functionalization with unconventional, fully inorganic electrophiles like main-group element halogenides $EX_3$ (E = B, Al, Ga, P).[15] Furthermore, these BN-amides were recently shown to serve as precursors for group 11 metal complexes, wherein the 1,2-azaborine acts as a *m*-terphenyl analogue, *i.e.* an anionic nitrogen ligand.[17]

The BN/CC isosterism can be extended from benzene/azaborines to more complex systems such as the alkaloid isoquinoline and its isoelectronic BN-congeners 1,2,3-diazaborines (DABs, Fig. 1b).[18,19] The presence of a second, endocyclic $N_\beta$ atom, bearing a free, exocyclic lone pair, endows DABs with an additional Lewis-basic functionality (Fig. 2a).[19,20] Their reduced aromaticity compared to the related 1,2-azaborines renders the boron atom more susceptible to nucleophilic attack and formation of $sp^3$-hybridized boron species.[19,21,22]

The first DAB syntheses date back to Dewar and Dougherty in 1962 and research has been primarily focused on hemiboronic acid derivatives ever since.[18] The standard procedure for the preparation of these benzoid, hemiboronic acid DABs is the condensation of 2-formylphenyl boronic acid (2-FPB) with hydrazine.[19,23] The choice of hydrazine derivative irreversibly predetermines the *N*-substituent in most cases and is limited by the availability and hazardous nature of the respective hydrazines. While our group recently presented a convenient method for the *B*-functionalization of established hemiboronic acid DABs,[21] options to subsequently modify the *N*-substituent are scarce. Herein, we explore an approach to late-stage *N*-functionalization with organic and inorganic substrates by isolation of nucleophilic DAB alkali metal amides. In contrast to the straightforward *N*-functionalization of related 1,2-azaborine alkali metal salts *via* salt metathesis reactions,[13–16] subsequent reactivity studies of these DAB amides revealed an intricate, dualistic behavior as *N*-nucleophiles, as well as anionic diazo ligands for formation of coinage metal complexes due to the incorporation of the second nitrogen atom.

## Results and discussion

### Synthesis of the precursor 2H

Considering the potential biological applications of DABs and the inherent hazards associated with the parent hydrazine ($N_2H_4$), we began by developing an alternative synthesis of the DAB **1H** on a large laboratory scale. Starting from the relatively non-hazardous *N-tert*-butyloxy-carbonyl (Boc) hydrazine, the Boc-substituted DAB **1Boc** was obtained in excellent yield through an adapted standard procedure (Scheme 1).

Subsequent acidic deprotection with neat trifluoroacetic acid (TFA) quantitatively afforded DAB **1H**, which was then converted into its corresponding trimethylsilyl (TMS) ether, following a general procedure previously reported by our group.[21,24] Owing to its low molecular weight, compound **2H** was separated from the byproduct *N*-(trimethylsilyl)acetamide by fractional sublimation and obtained in overall good yields.

### Deprotonation of 2H

Given that subsequent *B*-functionalization of **2H** necessitates the use of organometallic reagents (*e.g.* RLi, RMgBr), we investigated the response of **2H** toward basic conditions. The

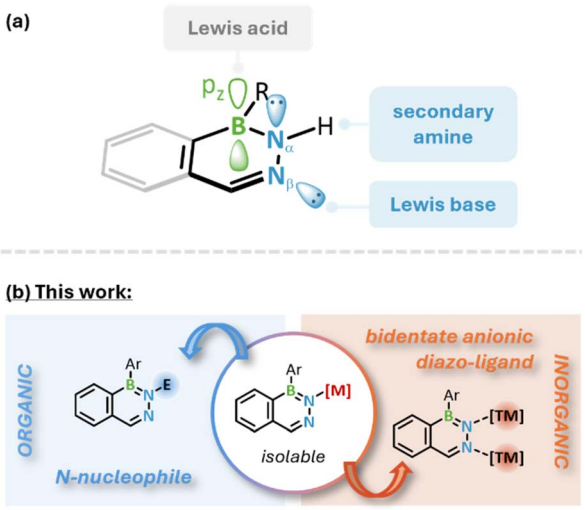


Fig. 2 (a) General DAB scaffold with a secondary amine function at $N_\beta$ and Lewis acidic and Lewis basic centers; (b) Reactivity studies presented herein: Preparation of alkali metal diazaboramides and their reaction as *N*-nucleophile or bidentate anionic diazo ligand.

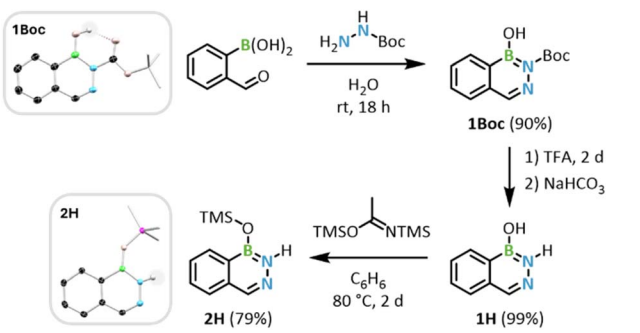


Scheme 1 Synthesis of **2H** *via* Boc-substituted DAB **1Boc** and deprotection to **1H** (Boc = *N-tert*-butyloxycarbonyl; TFA = trifluoroacetic acid; TMS = trimethylsilyl). Inset: solid-state structures of **1Boc** (top) and **2H** (bottom).

reaction of **2H** with lithium hexamethyldisilazide (Li[HMDS]) resulted in the formation of a colorless solid, which was identified as borazine **3** using high-resolution mass spectroscopy (HRMS) and 2D NMR spectroscopy (Scheme 2a). Compound **3** was isolated in a good yield of 72% and shows a broad $^{11}$B NMR resonance at 30.5 ppm, consistent with the presence of three sp$^2$-hybridized boron centers and its high molecular $C_{3h}$ symmetry. Due to its poor solubility in common aprotic solvents, no single crystals of **3** for XRD could be obtained. However, the formation of a borate decomposition product during workup serves as further constitutional proof of compound **3** (see ESI appendix, Fig. S85†). The poor solubility of **3** is likely attributed to extensive π–π stacking, further indicated by a very broad fingerprint band in the IR spectrum of **3** ($\tilde{\nu}$ = 967 cm$^{-1}$) and the compounds fibrous appearance.

Notably, **3** was also detected by $^{11}$B NMR spectroscopy as a side product when **2H** was treated with the more reactive amides Na[HMDS] and K[HMDS] (Scheme 2b). However, the main product in these reactions was identified as the putative borate **4M** with a broad $^{11}$B NMR resonance at 29.3 ppm and a sharp signal at −1.9 ppm, suggesting a lower molecular symmetry compared to that of **3**. In the case of **4K**, the solid-state structure was confirmed by single-crystal X-ray diffraction. While the borate formation proceeds within hours at ambient temperature, the subsequent B–O–B condensation and elimination of hexamethyldisiloxane (HMDSO) requires refluxing for several days. Solubility issues and partial decomposition during reflux prevented full characterization of **4M**, limiting analytics to *in situ* NMR spectra and single-crystal XRD (see ESI, Appendix†).

The reaction outcome is strongly influenced by the alkali metal employed, which suggests a varying nucleophilicity of the respective transient lithium or sodium and potassium DAB species **2M**. While **2Li** mainly trimerizes to the neutral borazine **3**, behaving as a mild nucleophile, its sodium and potassium congeners **2Na** and **2K** exhibit more pronounced nucleophilic character, leading to the formation of the diazaborinate **4M**. This reactivity trend parallels the reactivity of other metal organyls towards DABs, such as harsh organolithiums (RLi) and comparatively mild Grignard reagents (RMgBr).[21]

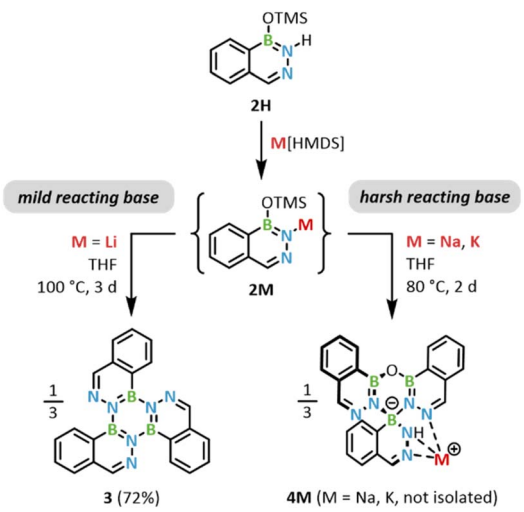


Scheme 2 Deprotonation of **2H** with Li[HMDS] to trimerization borazine product **3** (left) and with M[HMDS] (M = Na, K) to diazaborinate **4M** (right, HMDS = hexamethyldisilazide).

### *B*-Functionalization of 2H

Aryl-substituted DABs without sufficient steric protection are susceptible to attack by strong nucleophiles, leading to the formation of diazaborinates.[21] Upon the envisioned subsequent deprotonation, the aryl DAB amide products may exhibit moderate to strong nucleophilicity – depending on the alkali metal – and might therefore be prone to self-attack at a less-well-protected boron center. Thus, the kinetically stabilizing duryl substituent was chosen for the *B*-functionalization of **2H** over a smaller phenyl group. While duryl lithium is generally a suitable reagent for *B*-functionalization of DABs,[21] the inevitable simultaneous deprotonation of **2H** resulted in the formation of byproducts **3** and traces of **4Li**. We therefore chose durylmagnesium bromide, as the corresponding magnesium diazaboramide of **2H** was expected to be less reactive overall (Scheme 3, *cf.* general reactivity of RLi *vs.* RMgBr).

The reaction was monitored by $^{11}$B NMR spectroscopy after heating and prior to aqueous quenching. This revealed the highly selective conversion of **2H** to the intermediate tetrameric species **5**, resonating at 40.3 ppm, with no detectable diazaborinate byproducts (see ESI Appendix and Fig. S90†). Complex $^1$H NMR spectra prevented a full 2D NMR

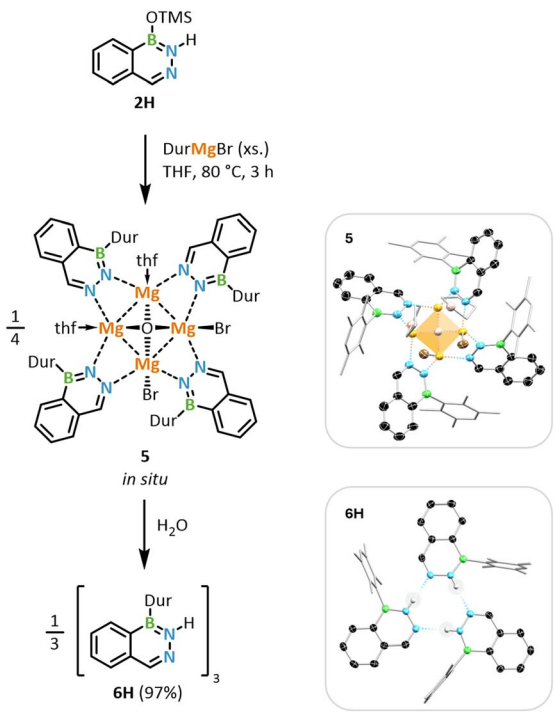


Scheme 3 Functionalization of **2H** with an excess of DurMgBr to form the μ-oxo[$Mg_4O$]-cluster **5**, followed by aqueous workup to obtain compound **6H** (Dur = 2,3,5,6-tetramethylphenyl). Byproducts: Dur-H, $MgBr_2$, 0.25 eq. $O(TMS)_2$, 0.5 eq. DurMg(OTMS). Insets: solid-state structures of **5** (top) and **6H** (bottom).

characterization of **5** and might be indicative of a Schlenk-like equilibrium in solution.[25–27] Solid-state XRD analysis of **5** unveiled an unusual μ-oxo[$Mg_4O$] cluster motif, which features an oxodianion $O^{2-}$ intercalated in the center of a [$Mg_4$] tetrahedron, originating from one OTMS-group of 0.25 equivalents **2H** (see ESI Appendix and Fig. S89†). The overall structural motif is remotely reminiscent of a Hauser base.[27] Four equivalents of the deprotonated DAB are μ-bridging four edges of the [$Mg_4$] tetrahedron *via* the diazo unit. The solid-state structure of **5** exhibits nearly identical N–Mg distances for both nitrogen atoms ($N_\alpha$–Mg 2.063(4) Å and $N_\beta$–Mg 2.090(4) Å), indicative of negative charge distribution across both N atoms. Similar μ-oxo [$Mg_4O$] structural motifs featuring NHC or triazolato ligands have been previously reported by Zhuang *et al.* or Mösch–Zanetti and coworkers, although examples remain rare.[28,29] Subsequent aqueous work-up gave the duryl-substituted DAB **6H** with secondary amine function in excellent yield of 97%. The $^{11}$B NMR resonance of **6H** at 36.9 ppm is in the typical region of aryl-substituted DABs and confirms the successful functionalization.[21,30] Compound **6H** trimerizes in the solid-state *via* intermolecular hydrogen bonds of the Lewis basic $N_\beta$ atom and the adjacent $N_\alpha$–H functionality.

### Deprotonation of 6H

A variety of bases were tested for the subsequent deprotonation of **6H** to the corresponding metalated diazaboramide. Attempts with *n*-butyllithium resulted in a complex product mixture, including competitive nucleophilic attack of *n*-butyllithium at the electrophilic aldimine position of the DAB. In contrast, employing the weaker base methyllithium or the sterically hindered tetramethylpiperidide lithium (LiTMP), Li[HMDS] as well as its heavier alkali metal congeners Na[HMDS] and K[HMDS] selectively afforded the desired diazaboramides **6M** (Scheme 4, top).

The heavier homologues **6Na** and **6K** slowly precipitated from concentrated benzene reaction mixture, allowing their isolation *via* filtration in a donor-free form and overall moderate yields. In contrast, **6Li** shows excellent solubility even in nonpolar solvents such as *n*-pentane. Hence clean separation from the corresponding protonated base byproduct is only feasible when equimolar amounts MeLi are employed, harnessing the formation of the gaseous byproduct $CH_4$. However, the high selectivity of the deprotonation reaction (Scheme 4, bottom inset) also encourages *in situ* functionalization reactions of **6M** (*vide infra*) without prior purification.

### Structures of 6M in solution

The successful deprotonation of **6H** was confirmed by the absence of the characteristic N–H resonance at 9.15 ppm in the *in situ* $^1$H NMR spectra (Scheme 4, bottom inset). No $^{11}$B NMR resonance was detected for all species **6M** in benzene, while a broad signal was observed in THF-$d_8$ at 37.4–37.9 ppm. This is indicative of a solvent-dependent aggregation, with benzene favoring higher-order aggregates. As the degree of aggregation usually highly influences the reactivity of organometallic species, this led us to further investigate the structures of **6M** in solution *via* diffusion-ordered spectroscopy (DOSY). Solubility

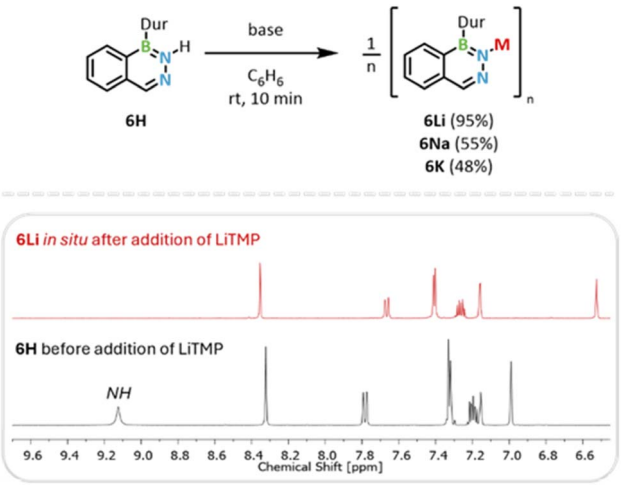


Scheme 4 Deprotonation of **6H** with alkali metal bases (M = Li: MeLi, LiTMP; M = Li, Na, K: M[HMDS]); $n(C_6H_6) = 4$, $n$(THF) = 2); bottom inset: *in situ* $^1$H NMR spectra before (black) and after (red) addition of LiTMP to a solution of **6H** in $C_6D_6$.

limitations restricted the $^1$H DOSY NMR measurements for isolated compounds **6Na** and **6K** to THF-$d_8$, whereas **6Li** was studied in both THF-$d_8$ and toluene-$d_8$. *In situ* experiments for **6Li** were permitted by the high selectivity of the reactions and the inert coordinative nature of the byproduct TMPH (see ESI, Fig. S92 and S93†). Significant differences in the diffusion coefficients of compound **6Li** in THF-$d_8$ and toluene-$d_8$ were found and confirm different aggregation states in both solvents. Molecular weights of **6Li**, **6Na**, and **6K** were determined by considering averaged aryl diffusion coefficients and estimated qualitative molecular shape, employing a method made available by Neufeld and Stalke.[31] Results are summarized in Table 1 and fit a tetrameric structure of **6Li** in the non-coordinating solvent toluene, whereas all diazaboramides **6M** (M = Li, Na, K) adapt dimeric structures upon dissolution in the coordinating solvent THF.

### Structures of 6M in the solid state

Complementary to the DOSY NMR studies in solution, single-crystal XRD experiments were conducted on all diazaboramides **6M** (M = Li, Na, K) to investigate their structures in the solid state. For **6Li**, single crystals were grown from both benzene and THF, revealing identical aggregation states as

Table 1 Results of the $^1$H DOSY NMR experiments for **6M** (M = Li, Na, K) in THF-$d_8$ or toluene-$d_8$, 25 °C. Averaged diffusion coefficient $\bar{D}$, derived aggregate and difference of the calculated molecular weight (MW) to the theoretical MW for each aggregate. For details see ESI, Table S2

| No. | Solvent | $\bar{D}$ [m$^2$ s$^{-1}$] | Aggregate | $\Delta MW_{calc}$ |
|---|---|---|---|---|
| **6Li** | Toluene-$d_8$ | $5.415 \times 10^{-10}$ | Tetramer | 2% |
| **6Li** | THF-$d_8$ | $7.304 \times 10^{-10}$ | Dimer | 8% |
| **6Na** | THF-$d_8$ | $8.102 \times 10^{-10}$ | Dimer | 4% |
| **6K** | THF-$d_8$ | $8.015 \times 10^{-10}$ | Dimer | 8% |

observed in solution (tetrameric in benzene and dimeric in THF, Fig. 3a and b). Upon dimerization in THF, **6Li** stabilizes itself *via* μ-coordination of the Lewis basic $N_\beta$ atom to the Li atom of the second DAB unit (Fig. 3a).

The remaining exposed coordination sides of both Li atoms are saturated by THF complexation. Compared to the μ-oxo $[Mg_4O]$ cluster **5**, the N→M metal interaction in **6Li** is slightly more unsymmetrical, with N2···Li1′ and N1···Li1 bond distances of 2.077(4) Å and 2.000(3) Å, respectively, suggesting a more covalent $N_\alpha$–Li and dative $N_\beta$→Li bond, similar to compound **6BCat** (*vide infra*). The B1═N1 bond length of 1.422(3) Å in **6Li** is slightly elongated compared to that of the precursor **6H** (*cf.* 1.400(3) Å), indicating the redistribution of electron density from the B═N bond to the alkali metal. With a B1–N1–N2–C1 torsion angle of 1.6(3)° the DAB unit is still approximately planar, however, the central $Li_2N_4$ chelate is heavily twisted to accommodate the Li coordination number of four. In benzene, **6Li** adopts a tetrameric structure featuring a $Li_4$ core with a distorted tetrahedral geometry (Li···Ct···Li angles ranging from 102.78° to 124.45°, Fig. 3b). While in **5**, the four DABs bridge the edges of the regular $Mg_4$ tetrahedron, in **6Li** all DAB ligands reside closer above the faces than the edges of the tetrahedron. This arrangement is reminiscent of the cubane-type tetrameric structure observed for methyllithium in the solid state.[32] Analogous to $[MeLi]_4$, the high solubility of **6Li** in non-polar solvents is explained by its spherical geometry, as the polar $Li_4$ core is effectively shielded by the organic DAB periphery.

Fig. 3c shows the interaction of a single DAB segment with the tetrameric $M_4$ cores in all three diazaboramides **6M** (M = Li, Na, K) in benzene. While for **6Li** only one molecule is found in the asymmetric unit, for **6Na** and **6K** three molecules form the

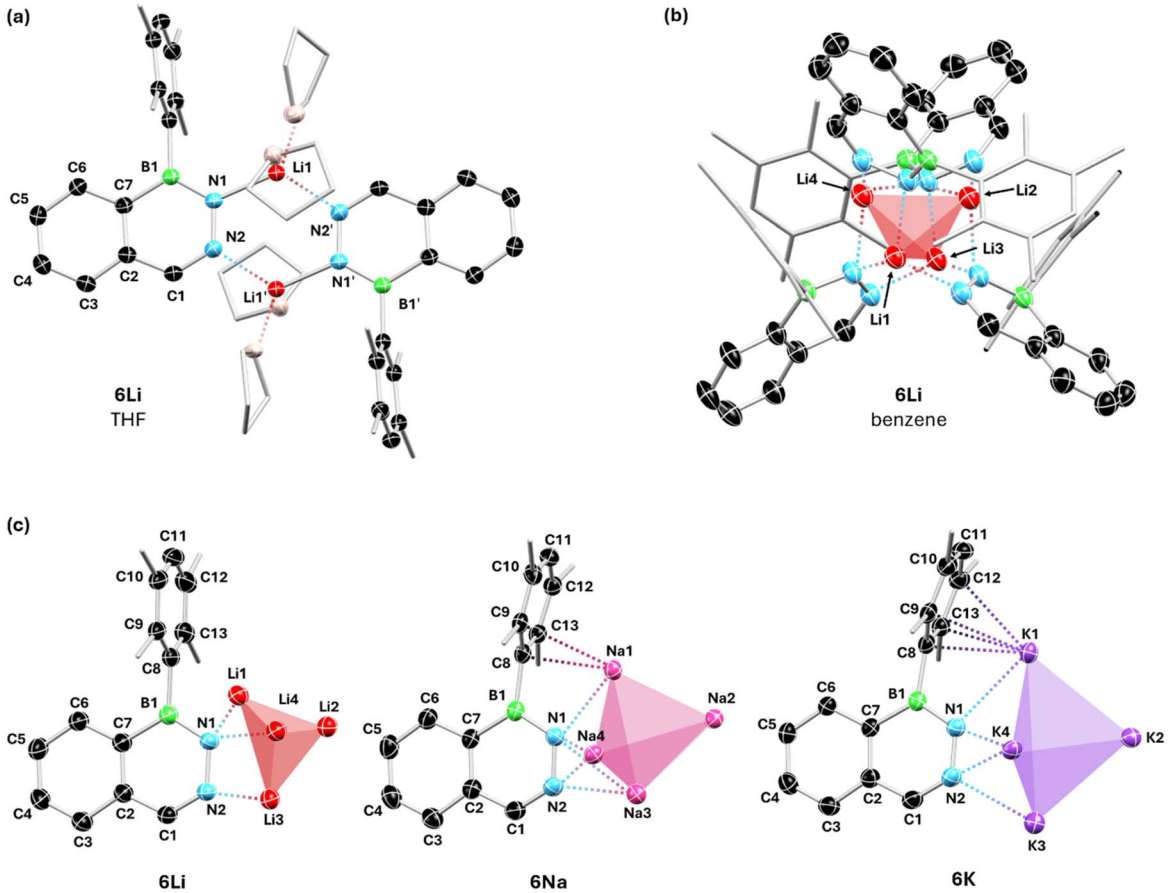


Fig. 3 Molecular structures of (a) dimeric **6Li** from crystallization in THF, (b) tetrameric **6Li** from crystallization in benzene and (c) view of a single DAB segment of each **6Li**, **6Na** and **6K** from crystallization in benzene and its interaction with the four metal centers in the tetrameric cluster structures (ellipsoids drawn at 50% probability). Selected bond lengths (Å) and angles (°) of **6Li** in THF (a): B1–N1 1.422(3), N1···Li1 2.000(3), N2···Li1′ 2.077(4), N1–N2 1.380(2), N2–C1 1.315(3), B1–N1–N2–C1 1.6(3), Li1···N1···N2···Li1′ 42.8(2). Selected bond lengths (Å) and angles (°) of **6Li** in benzene (b and c, left): B1–N1 1.414(2), N1–N2 1.4076(19), N2–C1 1.300(2), N1–Li1 2.068(3), N1–Li4 2.061(3), N1–Li3 2.542(3), N2–Li3 1.985(3), B1–N1–N2–C1 2.3(2), Li1···Li2 3.045(4), Li2···Li3 2.667(4), Li3···Li4 3.020(4), Li4···Li1 2.712(4). Selected bond lengths (Å) and angles (°) of **6Na** in benzene (c, middle): (A) B1–N1 1.410(3), N1–N2 1.396(3), N2–C1 1.304(3), N1–Na1 2.504(2), N1–Na4 2.483(2), N1–Na3 2.768(2), N2–Na3 2.366(2), N2–Na4 2.666(2), B1–N1–N2–C1 2.8(3), Na···Na 3.1068(15); (B) B1–N1 1.418(3), N1–N2 1.396(3), N2–C1 1.303(3), N1–Na1 2.476(2), N1–Na4 2.943(2), N1–Na3 2.450(2), N2–Na3 2.403(2), N2–Na4 2.539(2), B1–N1–N2–C1 1.6(3), Na···Na 3.1328(14). Selected bond lengths (Å) and angles (°) of **6K** in benzene (c, right): (A) B1–N1 1.415(3), N1–N2 1.394(2), N2–C1 1.306(3), N1–K1 2.9761(18), N1–K4 3.0373(18), N1–K3 2.8027(18), N2–K3 2.8650(19), N2–K4 2.6861(19), B1–N1–N2–C1 1.0(3), K1···K2 3.5821(7), K2···K3 4.0834(6), K3···K4 3.5821(7), K4···K1 4.0834(6); (B) B1–N1 1.415(3), N1–N2 1.382(3), N2–C1 1.305(3), N1–K1 2.8921(18), N1–K4 2.8009(18), N2–K4 2.7827(19), N2–K3 2.767(2), B1–N1–N2–C1 1.0(3), K1···K2 3.6675(7), K2···K3 3.6529(7), K3···K4 3.6675(7), K4···K1 3.6529(7).

crystallographic asymmetric unit with significantly different bond parameters for the $M_4$ core. For example, for the central $K_4$ motif in **6K**, a molecule with a slightly distorted tetrahedral arrangement (K···Ct···K 102.26° to 125.12°) analogous to **6Li** and two molecules with a strongly distorted tetrahedron closer to a butterfly-like structure (K···Ct···K 100.29° to 134.47°) are found. The deviation of **6Na** and **6K** from a spherical geometry accounts for their reduced solubility in nonpolar solvents. As a result of the distortion, more μ and, unlike **6Li**, additional η Ar···M interactions between the duryl substituent and the metal center are found for **6Na** and **6K**. These η interactions are also indicated by a broadening of the $^1$H NMR resonances of the *o*-$CH_3$ groups in diluted $C_6D_6$ solution directly after addition of the base. For the sodium compound, a $\eta^1$-to-$\eta^3$-like coordination was found, while the metal–aryl interaction in the potassium congener is more pronounced, resembling $\eta^3$-to-$\eta^5$ coordination. Similar metal–aryl interactions are also observed for the related alkali metal salts of 1,2-azaborines.[15]

### Reactivity of 6M as organic nucleophile

In analogy to the related metalated 1,2-azaborines,[15] we expected salt metathesis reactions of the diazaboramides **6M** with main-group-element halogenides to proceed relatively straightforwardly and yield the corresponding *N*-functionalized products. However, upon equimolar reaction of **6M** (M = Li, K) with various substrates such as $ECl_3$ (E = B, Al, Ga, P) or $PhBBr_2$, complex mixtures of multiple species were observed, and no product was isolable. One reason was suspected to be the comparatively lower steric demand of the DAB amides, enabling two- or threefold substitutions. This prompted us to switch to the monohalogenated borane CatBBr (Cat = catechol), as well as more conventional electrophiles such as methyl iodide or trimethylsilyl chloride (Scheme 5).

In the cases of TMSCl and MeI, the reaction was performed by *in situ* deprotonation of **6H** to **6K** and subsequent addition of the electrophile in a convenient one-pot synthesis. While the reaction of **6K** with CatBBr proceeded immediately at room temperature, affording the desired nucleophilic substitution product **6BCat**, the analogous reactions with trimethylsilyl chloride or methyl iodide, to **6TMS** and **6Me** respectively, required longer reaction times. Moreover, no reaction was observed for the latter when the less reactive **6Li** was used. In the case of **6BCat**, the $^{11}$B NMR resonance of the DAB boron atom is significantly downfield shifted compared to **6H** and detected as very broad singlet at 43.3 ppm due to quadrupolar broadening by the second boron nucleus (*cf.* $\delta(^{11}B, \mathbf{6H}) = 36.9$ ppm). A resonance at 9.8 ppm, corresponding to the catechol borane moiety, confirms the successful *N*-borylation and is in line with a weak adduct *via* the Lewis basic $N_\beta$ atom of a second DAB. Single crystal XRD analysis confirmed the dimeric nature of **6BCat** (Scheme 5, inset), reminiscent of the solid-state structure of **6Li** in THF (*vide supra*). Similar to **6Li**, the $N_\beta \rightarrow$**BCat** bond is significantly elongated compared to the $N_\alpha$–**BCat** bond (*cf.* 1.6137(15) Å *vs.* 1.5466(15) Å), supporting the dative character of the bond. The central DAB ring in **6BCat** is distorted from planarity

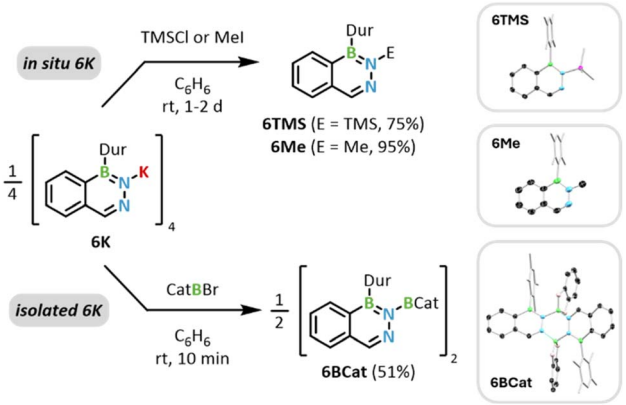


Scheme 5 *N*-Functionalization of **6M** to **6E** with electrophiles. Top: methyl iodide (MeI) and trimethylsilyl chloride (TMSCl), bottom: CatBBr (Cat = catechol). Inset: solid state structures of **6TMS**, **6Me** and dimeric **6BCat**.

by a torsion angle of 10.99(16)° for the B1–$N_\alpha$–$N_\beta$–C1 unit, either due to geometric strain in dimeric **6BCat** or a significantly diminished aromaticity caused by the electron withdrawing effect of the BCat substituent.

The successful preparation of **6E** (E = TMS, Me, BCat) is encouraging for future utilization of the DAB amides **6M** in late-stage *N*-functionalization, following the example of the 1,2-azaborines.[13–16] However, the complex reactions observed with $ECl_3$ mark a substantial difference to the 1,2-azaborine systems and motivated us to investigate the electronic situation in the deprotonated DAB amide anion $\mathbf{6}^-$ by means of density functional theory (DFT) calculations. Computations were performed using the Gaussian 16 program package[33] with the ωB97X-D[34] functional in combination with the def2-SVP[35] basis set. Fig. 4 depicts the frontier molecular orbitals (FMOs) of $\mathbf{6}^-$ alongside those of a corresponding, hypothetical azaborine anion $\mathbf{7}^-$.

For $\mathbf{7}^-$, the reactivity is primarily governed by the lone-pair character of the HOMO−1, which confers σ-donor character to the N atom and enables its classical nucleophilic behavior. In contrast, the HOMO of $\mathbf{6}^-$ displays two antiphasic σ(N) orbitals. The substantial partial localization at the $N_\beta$-atom provides further insight into the challenges encountered with more reactive electrophiles such as $ECl_3$, as it also imparts nucleophilic character to the $N_\beta$ atom.

### Reactivity of 6M as a monoanionic ligand

The shape and phase of the HOMO of $\mathbf{6}^-$ suggest that the DAB amide possesses the prerequisites to function as bidentate, monoanionic σ-donor ligand for transition-metal complexation. Due to the localization of the LUMO at the organic periphery of the backbone, $\mathbf{6}^-$ should thereby act exclusively as a donor ligand, lacking π–acceptor capability. This FMO situation is reminiscent of well-studied pyrazolato ($pz^-$) ligands ($\mathbf{8}^-$, Fig. 4), which are renowned for their coordination chemistry with monovalent coinage metals (TM = Cu, Ag, Au).[36] Their $[TM(pz)]_n$ complexes, mostly adopting trimeric, cyclic structures ($n$ = 3), have garnered significant interest due to their

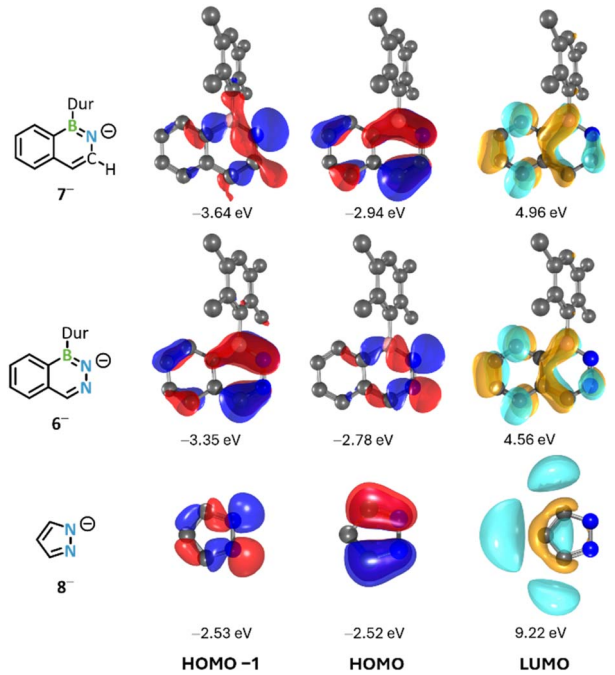


Fig. 4 HOMO−1 and FMOs of the free monoanions $6^-$ and $7^-$, as well as the pyrazolato ($pz^-$) anion $8^-$ (ωB97X-D[34]/def2-SVP[35]/isovalue 0.10 e Å$^{-3}$).

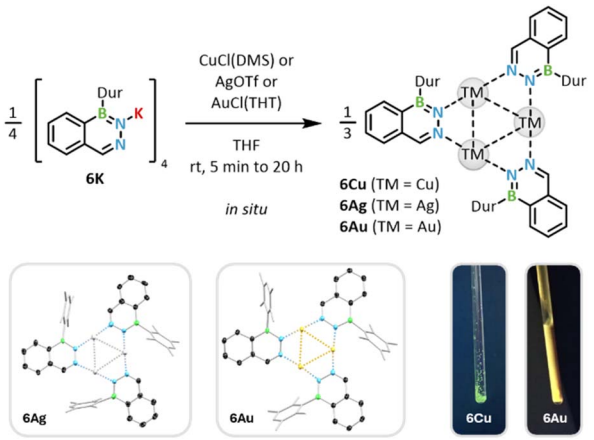


Scheme 6 Reaction of **6K** with copper(I) chloride dimethylsulfide complex, silver(I) triflate or gold(I) chloride tetrahydrothiophene to trimeric complexes **6TM** (DMS = dimethylsulfide, THT = tetrahydrothiophene, TM = Cu, Ag, Au). Insets: Solid-state structures of **6Ag** and **6Au** (left) and luminescent NMR samples of **6Cu** and **6Au** under UV light (right).

luminescent properties and supramolecular chemistry, among others.[37–39]

Therefore, we selected the highly Lewis-acidic coinage metal triad (TM = Cu, Ag, Au) to investigate the ligand properties of $6^-$. Given the potential formation of TM[HMDS]-coordinated side products upon *in situ* deprotonation of **6H** with M[HMDS], we reacted isolated **6K** with suitable metal(I) (pseudo) halides to afford the trimeric complexes **6TM** *via* salt metathesis (TM = Cu, Ag, Au, Scheme 6).

Formation of the Cu and Ag complexes **6Cu** and **6Ag**, respectively, proceeds within minutes. With Au, however, we observed the initial formation of an intermediate species, tentatively identified as the $\eta^2$ isomer by $^1$H NMR spectroscopy, which is slowly converted to μ-bridged complex **6Au** in solution (see ESI,† appendix Fig. S91†). *In situ* solution $^1$H DOSY NMR spectroscopy yielded similar hydrodynamic radii ($r_H$) for all complexes, consistent with coordination trimers in solution. The $^1$H NMR singlet resonance of the aldimine position generally serves as valuable spectroscopic probe for the electronic situation in the central DAB ring.[21] Deprotonation of **6H** to **6M** has no impact on the chemical shift of this resonance, consistent with a negative charge localization at the σ(N)-orbitals outside the DAB ring frame. However, upon TM-complexation, this singlet experiences a significant high-field shift of 1.0–1.4 ppm in THF-$d_8$ (*cf.* $\delta$($^1$H, **6K**) = 8.71 ppm *vs.* $\delta$($^1$H, **6Cu**) = 7.27 ppm), in line with the presence of an electron-rich transition metal. This shift is accompanied by deshielded, broadened $^{11}$B NMR resonances at 39.6–42.0 ppm due to the transfer of electron density into the $N_\alpha \rightarrow$ TM bond (*cf.* $\delta$($^{11}$B, **6K**) = 37.5 ppm).

While we were able to obtain small amounts of crystalline material of **6Ag** and **6Au** for single-crystal XRD experiments, confirming the formation of coordination trimers in the solid state (*vide infra*), all complexes **6TM** were primarily characterized *in situ* due to their limited stability in solution. Complexes **6Cu** and **6Ag** underwent clean decomposition to the protonated ligand **6H** and respective elemental metal, starting within 30 min of their NMR spectroscopic characterization. While **6Au** demonstrated comparatively higher stability, slow decomposition to colloidal gold, marked by the formation of a purple precipitate, was also observed after 20 h. Unfortunately, despite the intense green or yellow emission of the sample under UV irradiation (Scheme 6, inset), this instability limited investigation of the photophysical properties to an *in situ* study of complex **6Au** in solution (ESI, Fig. 93†). Given the instability of **6Au**, this UV-vis spectrum must be interpreted with caution (*cf.* Discussion section in ESI†).

Regardless of the limited stability of the complexes, we obtained single crystals of each derivative. However, in the case of **6Cu**, single-crystal XRD analysis was precluded by rapid oxidation of the crystals, despite careful coating in perfluorinated oil and fast transfer to a pre-cooled microscope slide, which is likely due to the comparatively low standard reduction potential ($E^0$) of $Cu^+$. In the silver and gold complexes **6Ag** and **6Au**, the TM–TM distances of 3.20–3.35 Å suggest intramolecular argento-/aurophilic interactions (Fig. 5a).[40] The DAB ligands adopt a symmetrical μ-bridging mode with nearly equivalent $N_\alpha \rightarrow$ TM and $N_\beta \rightarrow$ TM distances and slightly elongated B=N bonds, consistent with the electron-withdrawing effect of the TM. While the analogous pyrazolato ligand complexes often form stabilizing, intermolecular M···M interactions,[41] the duryl substituents, oriented perpendicular to the [μ-$N_2$TM]$_3$ core, preclude such interactions, which likely contributes to the low stability of **6TM** (Fig. 5b).

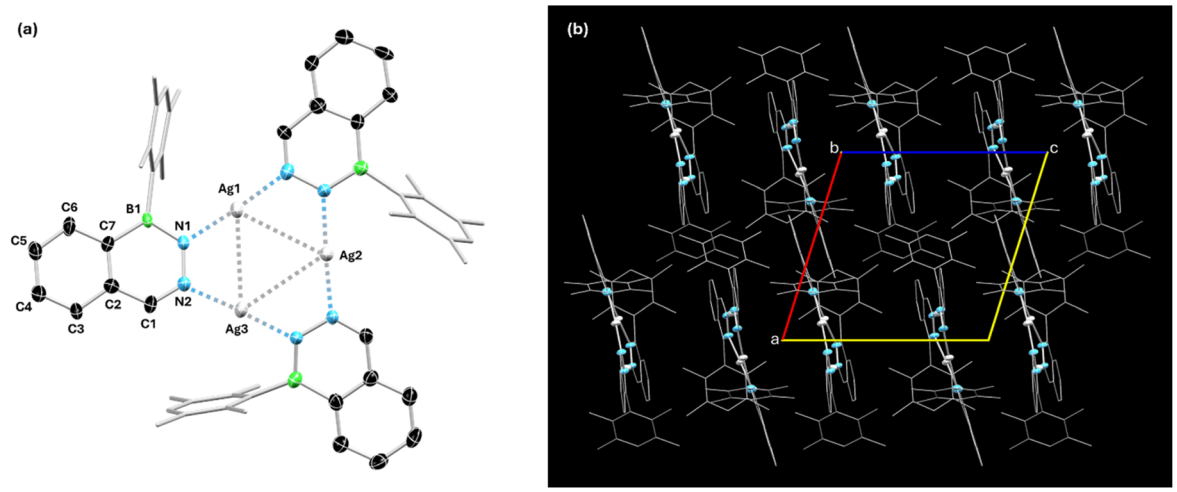


Fig. 5 (a) Molecular structure of trimeric complex **6Ag** in the solid state (ellipsoids drawn at 50% probability). Selected bond lengths (Å) and angles (°) of **6Ag**: B1–N1 1.410(9), N1–N2 1.367(8), N2–C1 1.289(9), N1–Ag1 2.074(7), N2–Ag3 2.071(8), Ag1···Ag2 3.3454(13), Ag2···Ag3 3.2805(13), Ag3···Ag1 3.2908(13), B1–N1–N2–C1 0.4(18), Ag3–N2–N1–Ag1 7.3(11). Selected bond lengths (Å) and angles (°) of **6Au**: B1–N1 1.414(7), N1–N2 1.390(5), N2–C1 1.298(6), N1–Au1 2.010(4), N2–Au3 2.016(4), Au1···Au2 3.2768(18), Au2···Au3 3.2475(16), Au3···Au1 3.1988(12), B1–N1–N2–C1 2.9(7), Au3–N2–N1–Au1 7.5(4). (b) Stacking of **6Ag** in the solid state.

## Conclusions

This study establishes a modular approach to the postsynthetic *N*-functionalization of *B*-aryl substituted diazaborines (DABs), drawing inspiration from established methods for 1,2-azaborines and employing a deprotonation strategy to access nucleophilic alkali metal amide DABs. Initial investigations explored potential side products during *B*-functionalization such as a borazine trimer or a metal borate, depending on the respective alkali metal base employed The intermediate species formed during *B*-functionalization with a Grignard reagent, prior to aqueous workup, was found to adopt a rare μ-oxo[$Mg_4O$] cluster structure in the solid state. The highly selective deprotonation of a secondary amine aryl DAB precursor enabled both *in situ* functionalization and isolation of the metalated DABs (M = Li, Na, K). Combined studies of their structures in the solid state and solution by XRD analysis and $^1$H DOSY NMR spectroscopy, respectively, revealed the formation of multimetallic aggregates.

Subsequent reactions of the DAB amides with mild electrophiles such as trimethylsilyl chloride or bromocatecholborane successfully demonstrated $N_\alpha$-functionalization. Computational studies suggested a parallel between the anionic diazo ligand character of the DAB amides and common pyrazolato ligands. This analogy was further substantiated by the formation of coordination trimers upon reaction of the DAB amide with group 11 metal(I) (pseudo)halides. In summary, this work showcases the dualistic reactivity of the alkali metal salts of DABs, highlighting their potential for both late-stage $N_\alpha$-functionalization and application as ligands in coordination chemistry.

## Data availability

The data supporting this article has been included as part of the ESI.† Crystallographic data for all compounds has been deposited at the CCDC under 2425624–2425639.

## Author contributions

H. B. conceived and designed the research program. L. W. wrote the manuscript, designed the studies and performed the experiments, with support from L. S. The crystallographic studies were conducted by K. R., T. W. and L. W. The quantum chemical calculations were performed by L. W. All authors have given approval to the final version of the manuscript.

## Conflicts of interest

This work was supported by the Julius-Maximilians-University Würzburg. There are no conflicts to declare.

## Acknowledgements

We are grateful to Dr Rian Dewhurst, Nele Wieprecht and Dr Ivo Krummenacher for insightful discussions and feedback on the manuscript. We also thank Laura Wolz for measurements of the $^1$H DOSY NMR spectra, Johannes Chorbacher for the photophysical experiments, Dr Dario Duwe and Johannes Chorbacher for starting materials and Dr Nils Schopper for measurement of a Raman spectrum.

## References

1 A. Stock and E. Pohland, *Ber. dtsch. Chem. Ges. A/B*, 1926, **59**, 2215–2223.
2 M. d. R. Merino-García, L. A. Soriano-Agueda, J. d. D. Guzmán-Hernández, D. Martínez-Otero, B. Landeros Rivera, F. Cortés-Guzmán, J. E. Barquera-Lozada and V. Jancik, *Inorg. Chem.*, 2022, **61**, 6785–6798.
3 R. Boese, A. H. Maulitz and P. Stellberg, *Chem. Ber.*, 1994, **127**, 1887–1889.

4 N. Wiberg and E. Wiberg, A. F. Holleman, *Lehrbuch der Anorganischen Chemie*, Walter de Gruyter, Berlin, 102th edn, 2007.
5 T. Yoshizaki, H. Watanabe and T. Nakagawa, *Inorg. Chem.*, 1968, **7**, 422–429.
6 R. Báez-Grez and R. Pino-Rios, *RSC Adv.*, 2022, **12**, 7906–7910.
7 B. Kiran, A. K. Phukan and E. D. Jemmis, *Inorg. Chem.*, 2001, **40**, 3615–3618.
8 H. Lee, M. Fischer, B. K. Shoichet and S.-Y. Liu, *J. Am. Chem. Soc.*, 2016, **138**, 12021–12024.
9 D. H. Knack, J. L. Marshall, G. P. Harlow, A. Dudzik, M. Szaleniec, S.-Y. Liu and J. Heider, *Angew. Chem., Int. Ed.*, 2013, **52**, 2599–2601.
10 C. R. McConnell and S.-Y. Liu, *Chem. Soc. Rev.*, 2019, **48**, 3436–3453.
11 D.-T. Yang, J. Zheng, J.-B. Peng, X. Wang and S. Wang, *J. Org. Chem.*, 2021, **86**, 829–836.
12 P. G. Campbell, A. J. Marwitz and S. Y. Liu, *Angew. Chem., Int. Ed.*, 2012, **51**, 6074–6092.
13 J. Pan, J. W. Kampf and A. J. Ashe III, *Organometallics*, 2004, **23**, 5626–5629.
14 J. Pan, J. W. Kampf and A. J. Ashe Ill, *Organometallics*, 2008, **27**, 1345–1347.
15 F. Lindl, A. Lamprecht, M. Arrowsmith, E. Khitro, A. Rempel, M. Dietz, T. Wellnitz, G. Bélanger-Chabot, A. Stoy, V. Paprocki, D. Prieschl, C. Lenczyk, J. Ramler, C. Lichtenberg and H. Braunschweig, *Chem. - Eur. J.*, 2023, **29**, e202203345.
16 H. Lee, M. Alvarado, S. Ingram, B. Li and S. Y. Liu, *Synlett*, 2023, **34**, 2169–2174.
17 A. Lamprecht, F. Lindl, L. Endres, I. Krummenacher and H. Braunschweig, *Chem. Commun.*, 2023, **59**, 10149–10152.
18 M. J. S. Dewar and R. C. Dougherty, *J. Am. Chem. Soc.*, 1962, **84**, 2648–2649.
19 M. Z. H. Kazmi, J. P. G. Rygus, H. T. Ang, M. Paladino, M. A. Johnson, M. J. Ferguson and D. G. Hall, *J. Am. Chem. Soc.*, 2021, **143**, 10143–10156.
20 M. Stojanović and M. Baranac-Stojanović, *J. Org. Chem.*, 2016, **81**, 197–205.
21 L. Wüst, J. Chorbacher, T. Wellnitz, S. Nees, H. Helten and H. Braunschweig, *Chem. Sci.*, 2025, DOI: **10.1039/D5SC01500F**.
22 E. A. Sarina, M. M. Olmstead, D. Kanichar and M. P. Groziak, *Acta Crystallogr., Sect. C:Cryst. Struct. Commun.*, 2015, **71**, 1085–1088.
23 J. P. M. António, J. I. Carvalho, A. S. André, J. N. R. Dias, S. I. Aguiar, H. Faustino, R. M. R. M. Lopes, L. F. Veiros, G. J. L. Bernardes, F. A. da Silva and P. M. P. Gois, *Angew. Chem., Int. Ed.*, 2021, **60**, 25914–25921.
24 B. Roques and D. Florentin, *J. Organomet. Chem.*, 1972, **46**, C38–C40.
25 G. S. Silverman and P. E. Rakita, *Handbook of Grignard Reagents*, CRC Press, 1996.
26 W. Schlenk and W. Schlenk Jr, *Ber. Dtsch. Chem. Ges. B*, 1929, **62**, 920–924.
27 R. Neufeld, T. L. Teuteberg, R. Herbst-Irmer, R. A. Mata and D. Stalke, *J. Am. Chem. Soc.*, 2016, **138**, 4796–4806.
28 Y. Zhuang, Y. Qian, D. Tu, Y. Li, J. Liu, L. Shen and D. Wu, *Chem. - Eur. J.*, 2021, **34**, 3443–3447.
29 N. C. Mösch-Zanetti, M. Ferbinteanu and J. Magull, *Eur. J. Inorg. Chem.*, 2002, **4**, 950–956.
30 F. Lindl, S. Lin, I. Krummenacher, C. Lenczyk, A. Stoy, M. Müller, Z. Lin and H. Braunschweig, *Angew. Chem., Int. Ed.*, 2019, **58**, 338–342.
31 R. Neufeld and D. Stalke, *Chem. Sci.*, 2015, **6**, 3354–3364.
32 E. Weiss and G. Hencken, *J. Organomet. Chem.*, 1970, **21**, 265–268.
33 M. J. Frisch, G. W. Trucks, H. B. Schlegel, G. E. Scuseria, M. A. Robb, J. R. Cheeseman, G. Scalmani, V. Barone, G. A. Petersson, H. Nakatsuji, X. Li, M. Caricato, A. V. Marenich, J. Bloino, B. G. Janesko, R. Gomperts, B. Mennucci, H. P. Hratchian, J. V. Ortiz, A. F. Izmaylov, J. L. Sonnenberg, D. Williams-Young, F. Ding, F. Lipparini, F. Egidi, J. Goings, B. Peng, A. Petrone, T. Henderson, D. Ranasinghe, V. G. Zakrzewski, J. Gao, N. Rega, G. Zheng, W. Liang, M. Hada, M. Ehara, K. Toyota, R. Fukuda, J. Hasegawa, M. Ishida, T. Nakajima, Y. Honda, O. Kitao, H. Nakai, T. Vreven, K. Throssell, J. J. A. Montgomery, J. E. Peralta, F. Ogliaro, M. J. Bearpark, J. J. Heyd, E. N. Brothers, K. N. Kudin, V. N. Staroverov, T. A. Keith, R. Kobayashi, J. Normand, K. Raghavachari, A. P. Rendell, J. C. Burant, S. S. Iyengar, J. Tomasi, M. Cossi, J. M. Millam, M. Klene, C. Adamo, R. Cammi, J. W. Ochterski, R. L. Martin, K. Morokuma, O. Farkas, J. B. Foresman and D. J. Fox, *Gaussian 16 Revision C.01*, Gaussian, Inc., Wallingford CT, 2019.
34 J.-D. Chai and M. Head-Gordon, *Phys. Chem. Chem. Phys.*, 2008, **10**, 6615–6620.
35 F. Weigend and R. Ahlrichs, *Phys. Chem. Chem. Phys.*, 2005, **7**, 3297–3305.
36 J. Elguero and I. Alkorta, *Molecules*, 2020, **25**, 5108.
37 M. A. Omary, M. A. Rawashdeh-Omary, M. W. A. Gonser, O. Elbjeirami, T. Grimes, T. R. Cundari, H. V. K. Diyabalanage, C. S. P. Gamage and H. V. R. Dias, *Inorg. Chem.*, 2005, **44**, 8200–8210.
38 Y.-X. Chen, H. Yu, L. Wu, Y.-J. Tong, J. Xu, H. Pang, C. Wu, T. Tian and G. Ouyang, *Nat. Commun.*, 2024, **15**, 7356.
39 G. Yang and R. G. Raptis, *Inorg. Chem.*, 2003, **42**, 261–263.
40 M. A. Halcrow, *Dalton Trans.*, 2009, 2059–2073.
41 T. Grimes, M. A. Omary, H. V. R. Dias and T. R. Cundari, *J. Phys. Chem. A*, 2006, **110**, 5823–5830.